Journal of Alloys and Compounds 783 (2019) 555–564

Contents lists available at ScienceDirect

Journal of Alloys and Compounds

journal homepage: http://www.elsevier.com/locate/jalcom

Effects of Ni and Si additions on mechanical properties and serrated flow behavior in FeMoPCB bulk metallic glasses

Jing Zhou [a], Baoan Sun [b], Qianqian Wang [a], Qiuman Yang [a], Weiming Yang [c], Baolong Shen [a, c, *]

[a] School of Materials Science and Engineering, Jiangsu Key Laboratory for Advanced Metallic Materials, Southeast University, Nanjing 211189, China
[b] Institute of Physics, Chinese Academy of Sciences, Beijing 100190, China
[c] Institute of Massive Amorphous Metal Science, China University of Mining and Technology, Xuzhou 221116, China

ARTICLE INFO

Article history:
Received 29 October 2018
Received in revised form
25 December 2018
Accepted 28 December 2018
Available online 28 December 2018

Keywords:
FeNi-based BMGs
Large plasticity
Serrated flow behavior
Shear-band dynamics

ABSTRACT

A novel ductile $Fe_{56}Ni_{20}Mo_4P_{11}C_4B_4Si_1$ bulk metallic glass (BMG) with saturation magnetic flux density of 0.93 T, coercivity of 1.9 A/m and plastic strain of 7% was successfully synthesized in this work. Effects of Ni and Si additions on mechanical properties and serrated flow behavior of Fe-Mo-P-C-B BMGs were systematically investigated. It was found that the simultaneous additions of Ni and Si are effective to improve the plasticity of $Fe_{76}Mo_4P_{12}C_4B_4$ BMG as indicated by the increase in the plastic strain from 1.7% to 7%. Serrated flow behavior is not observed in $Fe_{76}Mo_4P_{12}C_4B_4$ BMG. However, the chaos state occurs in $Fe_{56}Ni_{20}Mo_4P_{12}C_4B_4$ BMG, and eventually the self-organized critical (SOC) behavior appears in $Fe_{56}Ni_{20}Mo_4P_{11}C_4B_4Si_1$ BMG. The stable shear-band dynamics leads to the formation of multiple shear bands, resulting in a complex deformation process follow the SOC dynamics. The improved plasticity might result from an increased number of potential shear transition zone sites, and a stronger tendency of forming shear band interactions. This work provides a perspective from serrated flow behavior to understand plastic deformation mechanism in Fe-based BMGs with different plasticity.

1. Introduction

Since the Fe-metalloid amorphous alloy was firstly developed in 1967 [1], Fe-based amorphous alloys have been drawing increasing attention due to their excellent soft magnetic properties such as high saturation magnetic flux density (B_s), low coercivity (H_c) and low core loss [2], and some of them have been used as magnetic core alloys [3–5]. For FeNi-based amorphous alloys, due to their high permeability, they have been used to partly substitute permalloys in sensors, magnetic shielding, springs, read-write heads of digital devices etc., under the trademark of Metglas 2826 MB [6]. However, the critical size as thin ribbons limited their more widely applications as three-dimensional micro parts. In 1995, Fe-based bulk metallic glass (BMG) was firstly synthesized in Fe-(Al, Ga)-metalloid system [7]. From then on, a large number of Fe-based BMGs have been developed with great efforts devoted by materials scientists and researchers [8–15]. Among them, some FeNi-based BMGs with good soft magnetic properties and superhigh strength have been developed [16,17]. Nevertheless, the glass-forming ability (GFA) was increased and the bulk metallic glasses were successfully prepared, the plasticity remained poor, which yet limited their potential applications as structural and functional materials.

In recent years, an amount of Fe-based BMGs with superhigh strength and some ductility have been developed by modifying alloy compositions [18–25]. It has been found that two methods are effective to improve plasticity of Fe-based BMGs. The first method is in situ formation of composites containing $Fe_{23}B_6$ or α-Fe second phases, which can prevent a single shear band from traversing through the specimen and promote the generation of multiple shear bands [19,22,24]. However, precipitation of the second phases usually deteriorates the soft-magnetic properties of ferromagnetic BMG because the magnetic domain will be pinned by these second phases [26,27]. The second method is to add metallic elements with high Poisson's ratio, such as Ni element, because Ni element exhibits higher Poisson's ratio, and high Poisson's ratio has been proven to be one of the important factors in designing a glassy

* Corresponding author. School of Materials Science and Engineering, Jiangsu Key Laboratory for Advanced Metallic Materials, Southeast University, Nanjing 211189, China.
E-mail address: blshen@seu.edu.cn (B. Shen).

https://doi.org/10.1016/j.jallcom.2018.12.331
0925-8388/

alloy to alleviate the brittleness [28,29]. A lot of researches have shown that substitution of Ni for Fe is effective to improve the plasticity and toughness in Fe-based BMGs [18,20,30], as Ni has higher Poisson's ratio than Fe [31]. In particular, the $Fe_{50}Ni_{30}P_{13}C_7$ BMG with high yield strength of 2250 MPa and a significant plastic strain larger than 20% has been synthesized, which is the largest value reported to date for Fe-based BMGs [29,30]. More importantly, both Fe and Ni are magnetic elements and thus it is expected that the ductile FeNi-based BMGs synthesized via the second method will possess relatively good magnetic properties.

In addition, the serration behavior during compressive tests has been proven to be a direct reflection of the mechanical properties for BMGs, and serration analysis is a convictive method to understand the dynamics of shear banding [32–39]. Here the serration refers to the repeated jerky stress drop on the loading curves, formed by avalanche and arrest of shear bands during deformation. Some statistics studies reveal that the shear bands in brittle and plastic BMGs would follow a chaotic behavior or a self-organized critical (SOC) behavior, where the serrated flow behavior falls in peak distribution or a power law distribution [32,40]. According to such understanding, the plastic deformation and shear-band dynamics of BMGs under different testing conditions [32,41–45] have been reasonably explained. However, statistical studies of serrations in Fe-based BMGs with different elements additions are still rare. Thus, it is important to reveal the origin of the different plasticity in Fe-based BMGs with different elements additions, and the relationship among serrated flow behaviors, shear-band dynamics and plasticity of Fe-based BMGs.

Recently, $Fe_{39}Ni_{39}B_{14.2}Si_{2.75}P_{2.75}Nb_{2.3}$ BMG with a high yield strength of 2850 MPa and large plasticity of 7.8% has been synthesized [46]. However, there is a strong demand for reducing materials cost through decreasing the content of the precious elements Nb, Ni and B. Motivated by the analyses mentioned above, the aim of the present study is to synthesize ductile Fe-based BMGs with high strength, good soft magnetic properties and low materials cost. After investigation of our previous work [47–50], the $Fe_{76}Mo_4P_{12}C_4B_4$ BMG was selected as the base alloy in this study because of its excellent soft magnetic properties and high strength. By adding Ni and Si elements in this base alloy, the $Fe_{56}Ni_{20}Mo_4P_{11}C_4B_4Si_1$ BMG with less amount of Ni and B elements and without Nb element was successfully synthesized, which exhibits excellent soft magnetic properties of high B_s of 0.93 T and low H_c of 1.9 A/m, as well as high yield strength of 2780 MPa. Effects of Ni and Si additions on the mechanical properties and serrated flow behavior of Fe-Ni-Mo-P-C-B-Si BMGs were investigated. The statistics results of this Fe-based BMGs system with different additions were systematically analyzed from the viewpoint of dynamics methods, which might shed light on understanding the relationship among serrated flow behavior, shear-band dynamics and plasticity of Fe-based BMGs.

2. Experimental

Alloy ingots of $Fe_{76-x}Ni_xMo_4P_{12-y}C_4B_4Si_y$ (x = 0, 10, 20; y = 0, 1, 2 at. %) were prepared by induction melting the mixture of high purity Fe, Ni and Mo metals, C, B and Si crystals and prealloyed Fe-P ingots under a high-purified argon atmosphere. The mass losses were less than 0.2 wt%. Ribbons with a width of 1.6 mm and thickness of 20 μm were prepared by single-roller melt spinning with a linear velocity for copper wheel of 40 m/s. Cylindrical rods with diameters of 1–2 mm were prepared by copper mold casting. The structure of rods was examined using X-ray diffraction (XRD, D8-Discover, Bruker) with Cu Kα radiation.

B_s under a maximum applied field of 800 kA/m was measured with a vibrating sample magnetometer (VSM, Lake Shore 7410). H_c was measured with a DC B-H loop tracer (RIKEN BHS-40) under a field of 800 A/m. All the ribbon samples for magnetic property measurements were annealed at the temperature of T_g-50 K for 600 s to reduce the influence of inner stress on soft magnetic properties through structural relaxation. The yield strength (σ_y) and the plastic strain (ε_p) were measured by compression testing with a mechanical testing machine at room temperature with a strain rate of 5×10^{-4} s^{-1}. Specimens for mechanical measurements were cut from the as-cast glassy rods with an aspect ratio of 2:1 (1 mm in diameter). The deformation behaviors and fracture surfaces were examined by scanning electron microscopy (SEM, Sirion 200, FEI).

3. Results and discussion

The structural results were obtained from the XRD measurements. Fig. 1 shows the XRD patterns of as-prepared $Fe_{76-x}Ni_xMo_4P_{12-y}C_4B_4Si_y$ (x = 0, 10 and 20; y = 0, 1 and 2 at. %) glassy rods with different Ni and Si contents and the corresponding critical maximum diameter for fully glass formation. The XRD patterns of all specimens exhibit broad diffraction maxima, which is characteristic of an amorphous structure. It is worthy to mention that the broad diffusive amorphous halo peak shifts to a lower diffraction angle with addition of Si element. The principal diffraction angle (2θ) gradually decreases from 44.9° for Si-free BMGs to 43.3° for Si-containing BMGs, indicating structural changes of these Fe-based BMGs with Si addition.

The critical maximum diameters (D_{max}) for fully glass formation for various Ni and Si additions in $Fe_{76-x}Ni_xMo_4P_{12-y}C_4B_4Si_y$ metallic glasses are listed in Table 1. It can be seen that the critical diameter of $Fe_{76-x}Ni_xMo_4P_{12-y}C_4B_4Si_y$ BMGs decreases to 1.5 mm with the substitution of 10 and 20 at. % Ni for Fe, then increases to 2 mm with the addition of 1 at. % Si element. However, excessive addition of Si degrades the GFA of alloys, and the critical diameter decreases to 1 mm with 2 at. % Si addition. It shows that addition of Ni element decreases the GFA, while proper addition of Si element is effective to improve the GFA. It has been reported that the large (Fe, Ni and Mo) and small (B, C and Si) atoms can form a reinforced “backbone” in the amorphous structure, which would suppress the crystallization and increase the GFA [49]. Additionally, by alloying with small amounts of Si element, the network-like structure may become much stronger because of the mixing enthalpies with large negative values between Si and Fe, Ni or Mo elements [49,51]. This two effectiveness would increase the stability of the undercooled liquid, resulting in the enhancement of the GFA in Si containing alloys.

In addition to the high GFA, the Fe-based BMGs exhibit excellent soft magnetic properties. Fig. 2 shows hysteresis loops of melt-spun $Fe_{76-x}Ni_xMo_4P_{12-y}C_4B_4Si_y$ ribbons measured with VSM. The inset in Fig. 2 shows the changes of B_s and H_c as a function of Ni and Si content. The B_s and H_c decrease gradually from 1.10 to 0.88 T and 1.8 to 1.0 A/m with the increasing Ni content from 0 to 20 at. %, respectively, then increase to 0.93 T and 1.9 A/m with 1 at. % addition of Si element. The decrease of B_s with increasing Ni content is caused by the lower magnetic moment of Ni (0.6 μ_B) compared with that of Fe (2.2 μ_B). However, the increase of B_s with the replacement of P by Si can be attributed to the increase of magnetic moment of Fe. It has been suggested that Si possesses a smaller number of outer electrons (2 electrons) compared with P (3 electrons). Consequently, the decrease of outer electrons reduces the probability of filling up 3d bands of Fe, resulting in a larger magnetic moment [47,52]. The reason for the slightly increase of H_c with 1 at. % Si addition may be attributed to the increase of internal stress resulting from larger atomic size of Si than P, B and C elements [47,53].

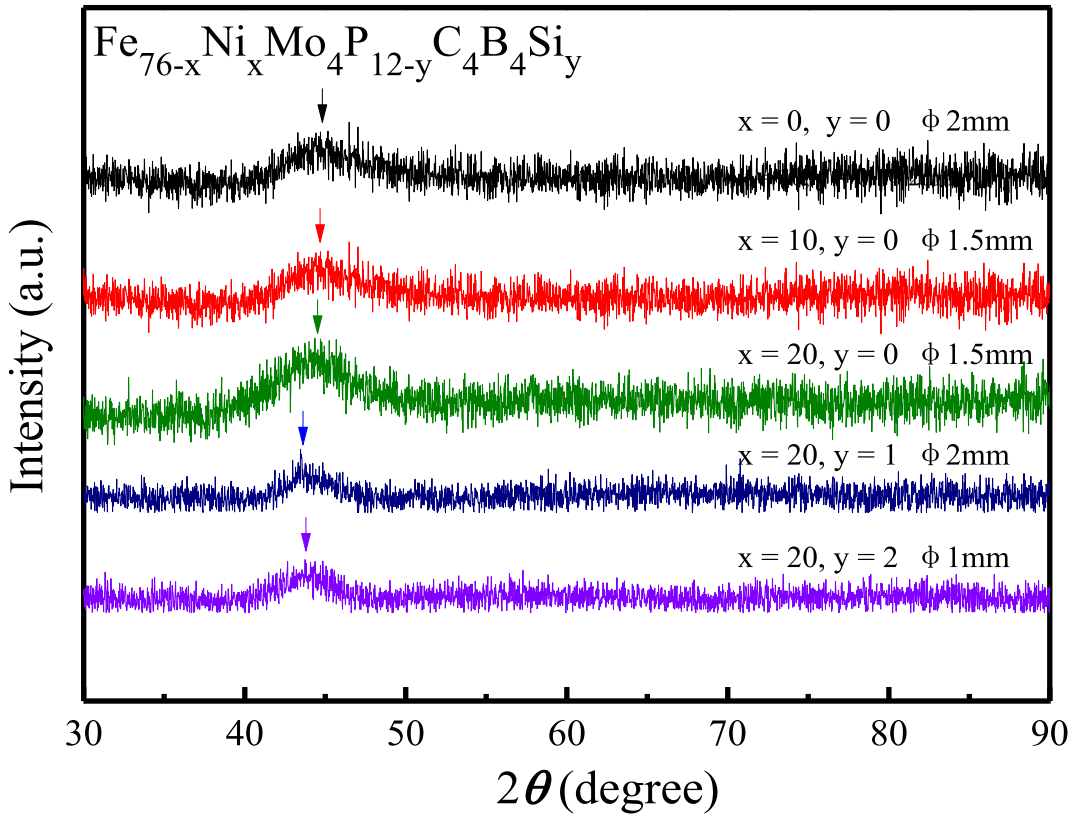

Fig. 1. XRD patterns of as-cast $Fe_{76-x}Ni_xMo_4P_{12-y}C_4B_4Si_y$ (x = 0, 10, 20; y = 0, 1, 2 at. %) BMGs.

Table 1
Maximum diameters, mechanical and magnetic properties of $Fe_{76-x}Ni_xMo_4P_{12-y}C_4B_4Si_y$ (x = 0, 10, 20; y = 0, 1, 2 at. %) metallic glasses.

Composition	D_{max} (mm)	Mechanical properties		Magnetic properties	
		σ_y (MPa)	ε_p (%)	B_s (T)	H_c (Am^{-1})
$Fe_{76}Mo_4P_{12}C_4B_4$	2	2875	1.7	1.11	1.8
$Fe_{66}Ni_{10}Mo_4P_{12}C_4B_4$	1.5	2700	3.6	1.07	1.5
$Fe_{56}Ni_{20}Mo_4P_{12}C_4B_4$	1.5	2680	5.9	0.88	1.0
$Fe_{56}Ni_{20}Mo_4P_{11}C_4B_4Si_1$	2	2780	7	0.93	1.9
$Fe_{56}Ni_{20}Mo_4P_{10}C_4B_4Si_2$	1	2890	0.3	0.91	3.5

In addition to the excellent soft magnetic properties, this Fe-based BMGs system exhibits good mechanical properties. Fig. 3 shows the engineering stress-strain curves of as-cast $Fe_{76-x}Ni_xMo_4P_{12-y}C_4B_4Si_y$ glassy rods tested under compression. All the samples exhibit high yield strength over 2500 MPa, whereas the plasticity strongly depends on the number of additional elements. For the metallic glasses with substitution of Ni for Fe from 0 to 20 at. %, the yield strength slightly decreases from 2875 to 2680 MPa, while plastic strain continuously increases from 1.7 to 5.9%. In contrast, the Si-containing metallic glasses show a non-monotonic dependence between mechanical properties and Si content. With an increase of Si addition content from 0 to 1 at. %, plastic strain increases from 5.9 to 7.0%, and then catastrophically fails without any plasticity with 2 at. % Si addition. The results show that modification of Fe to Ni concentration ratio and addition of Si element in $Fe_{76}Mo_4P_{12}C_4B_4$ BMG can effectively improve the room temperature compressive plastic deformability. Table 1 also summarizes the magnetic and mechanical properties of the $Fe_{76-x}Ni_xMo_4P_{12-y}C_4B_4Si_y$ metallic glasses.

To further characterize the deformation behavior of this Fe-based BMGs system with different addition of Ni and Si elements, we enlarge the stress-strain curves of three typical $Fe_{76}Mo_4P_{12}C_4B_4$, $Fe_{56}Ni_{20}Mo_4P_{12}C_4B_4$ and $Fe_{56}Ni_{20}Mo_4P_{11}C_4B_4Si_1$ BMGs with plastic strain of 1.7%, 5.9% and 7%, respectively, as shown in Fig. 4. Obviously, the mechanical responses of three Fe-based BMGs subjected to external stress are similar, which can be classified into three stages, i.e. the elastic deformation region (stageI), the steady-state plastic deformation region (stageII), and the stress-decreasing region (stage III). The plastic strain of different stages for three curves are 1.2%, 3.6%, 5.8% in stage II and 0.5%, 2.3%. 1.2% in stage III, respectively, which indicates that Fe-based BMGs with larger plasticity exhibit longer stage II. In addition, the serrated flow behavior also changed with the addition of Ni and Si elements. As seen in Fig. 4(d), $Fe_{76}Mo_4P_{12}C_4B_4$ BMG exhibits non-serrated-flow behavior during three stages. In contrast, the serrated-flow phenomena are evident on the stress-strain curves of $Fe_{56}Ni_{20}Mo_4P_{12}C_4B_4$ and $Fe_{56}Ni_{20}Mo_4P_{11}C_4B_4Si_1$ BMGs, as shown in Fig. 4(e) and (f), respectively. Even more interesting is the change of serration patterns in this Fe-based BMGs system with addition of Si element. In $Fe_{56}Ni_{20}Mo_4P_{12}C_4B_4$ BMG, the serration patterns are uniform and large. However, in $Fe_{56}Ni_{20}Mo_4P_{11}C_4B_4Si_1$ BMG, the serration patterns are much more complex with numerous small stress drops but fewer large ones. Although both curves display obvious serrated flow behavior, there are essential differences between them. The above results clearly suggest that the serrated flow behavior is composition dependent. The reasons of these behaviors will be discussed later.

Fig. 5 shows SEM images of deformed (before failure) and fractured (after failure) $Fe_{76}Mo_4P_{12}C_4B_4$, $Fe_{56}Ni_{20}Mo_4P_{12}C_4B_4$ and $Fe_{56}Ni_{20}Mo_4P_{11}C_4B_4Si_1$ BMGs. As shown in Fig. 5(a), only a single shear band along the direction of the largest shear stress (pointed

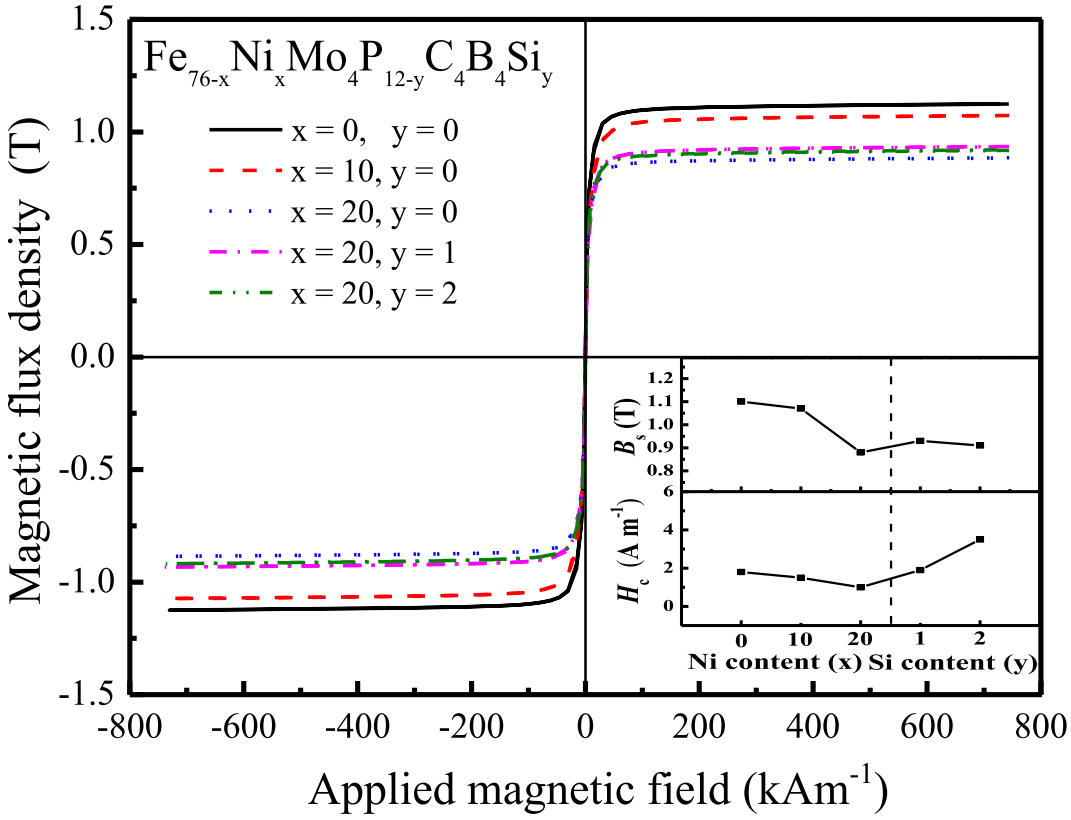

Fig. 2. Hysteresis loops of melt-spun $Fe_{76-x}Ni_xMo_4P_{12-y}C_4B_4Si_y$ (x = 0, 10, 20; y = 0, 1, 2 at. %) metallic glasses. The inset is the variations of B_s and H_c with different Ni and Si contents.

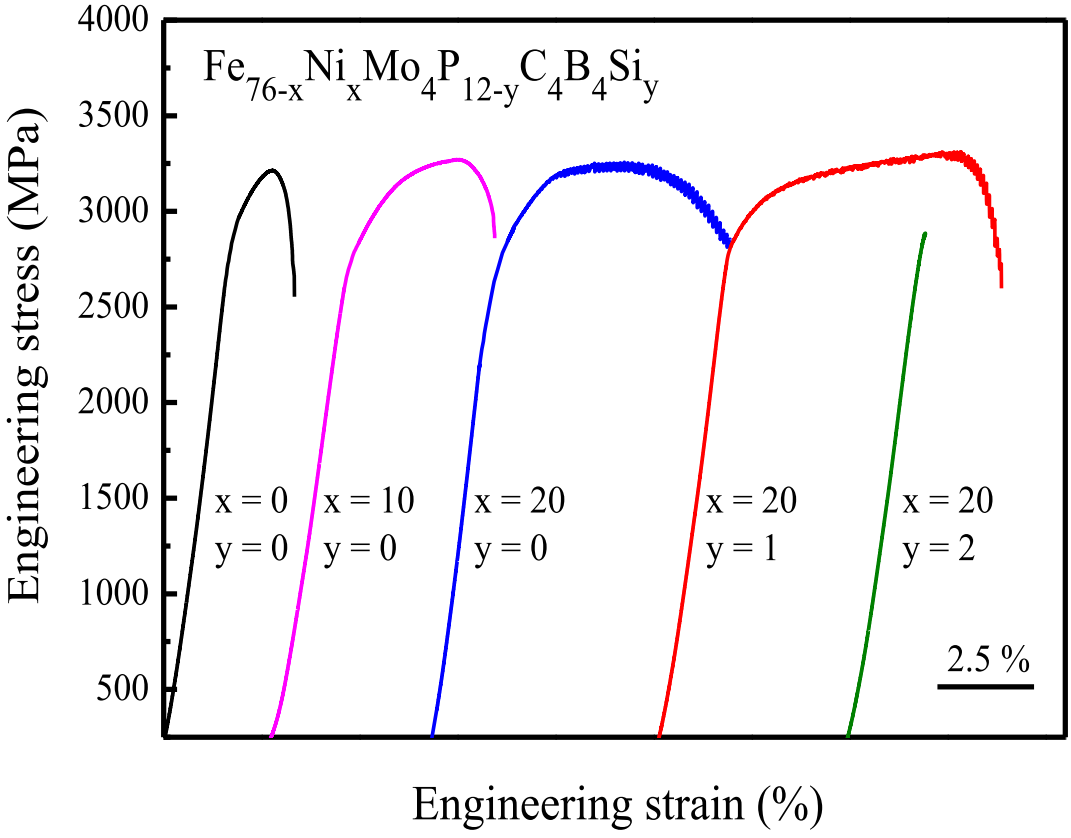

Fig. 3. Compressive stress-strain curves of as-prepared $Fe_{76-x}Ni_xMo_4P_{12-y}C_4B_4Si_y$ (x = 0, 10, 20; y = 0, 1, 2 at. %) BMGs.

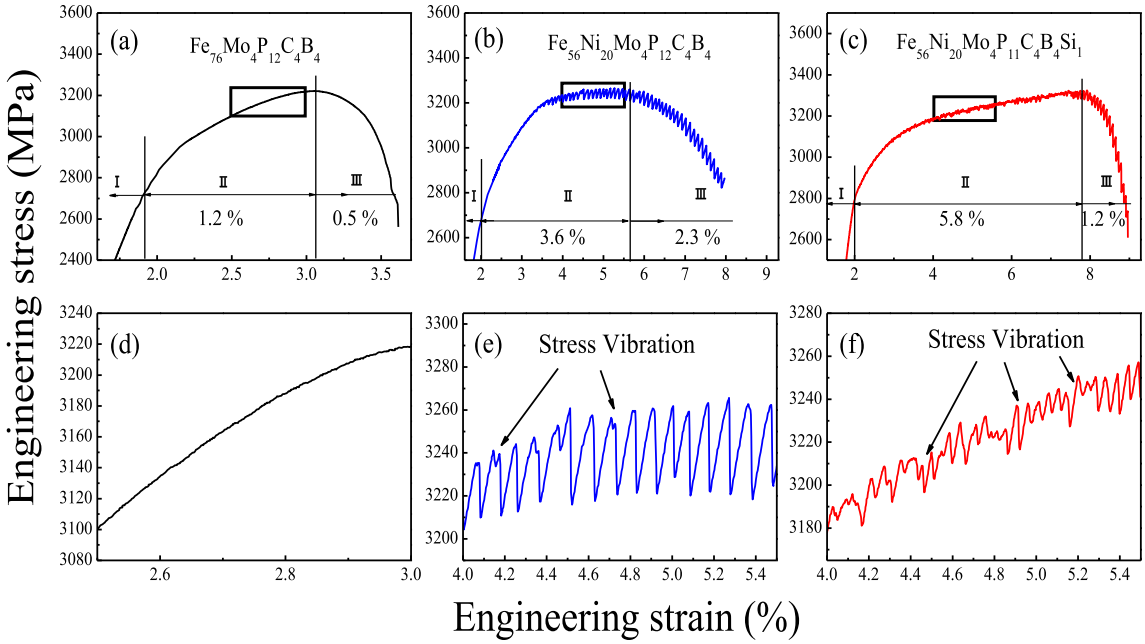

Fig. 4. Plastic strain regimes for (a) $Fe_{76}Mo_4P_{12}C_4B_4$ BMG, (b) $Fe_{56}Ni_{20}Mo_4P_{12}C_4B_4$ BMG and (c) $Fe_{56}Ni_{20}Mo_4P_{11}C_4B_4Si_1$ BMG. (d), (e) and (f) are the enlarged regions pointed by black rectangle in (a), (b) and (c) respectively.

by yellow arrow) can be observed in $Fe_{76}Mo_4P_{12}C_4B_4$ BMG. In $Fe_{56}Ni_{20}Mo_4P_{12}C_4B_4$ BMG (see Fig. 5(b)), a relatively large primary shear band and a few secondary shear bands (pointed by red arrow) appear on the lateral surface. In the $Fe_{56}Ni_{20}Mo_4P_{11}C_4B_4Si_1$ BMG (see Fig. 5(c)), a high density of secondary shear bands can be observed, which are paralleled to the existing primary shear band. Meanwhile, a large number of multiple shear bands are observed in Fig. 5(d) (enlarged region A in Fig. 5(c)). It is noticed that these shear bands are not straight in shape but interconnect with intersection, arresting or branching with each other, indicating the high resistance ability to propagation of shear bands. We further examined the fracture surface of $Fe_{56}Ni_{20}Mo_4P_{11}C_4B_4Si_1$ BMG. Fig. 5(e) shows robust plastic flow patterns on the fracture surface and multiple shear bands can also be found uniformly distributed on the lateral surface (region B in Fig. 5(e)). Furthermore, Fig. 5(f) shows the vein-like patterns (enlarged region C in Fig. 5(e)), which are the ductile fracture features and reveal the solidification of melted liquid flow with fast cooling process. The formation of multiple shear bands and the appearance of vein patterns can evidently verify the enhanced plasticity of $Fe_{56}Ni_{20}Mo_4P_{11}C_4B_4Si_1$ BMG.

Based on the above results, we try to explore the origin of enhanced plasticity due to the Ni and Si additions in this Fe-based BMGs system from viewpoint of dynamics methods. First, Fig. 4(a) and (b) show that the plastic strain of the $Fe_{76-x}Ni_xMo_4P_{12}C_4B_4$ continuously increases from 1.7 to 5.9% with addition of Ni element, accompanied with the appearance of serration behavior. The shear-band dynamics of $Fe_{76}Mo_4P_{12}C_4B_4$ BMG shown in Fig. 5(a) agrees with the non-serrated flow behavior, indicating that the sample deforms through a single shear band. It is known that non-serrated flow will happens during deformation under two conditions: one is the high speed of the primary shear band propagation, and the other is less secondary shear bands. However, the shear-band dynamics of the $Fe_{56}Ni_{20}Mo_4P_{12}C_4B_4$ BMG shown in Fig. 5(b) agrees with the large serration behavior, indicating that the deformation proceeds via the simultaneous operation of primary and secondary shear bands (multi-step shear banding), with each band contributing to the plasticity and none of them carrying enough strain to cause catastrophic failure [54]. Thus, the improved plasticity of this Fe-based BMGs system with addition of Ni element is obviously associated with the formation of secondary shear bands.

The reason why secondary shear bands can be activated with Ni addition could be understood from a perspective of inhomogeneity. At atomic scale, due to the structure and composition fluctuation, metallic glasses are inhomogeneous with the existence of potential shear transition zone (STZ) sites. When an external loading is applied to such materials, plastic deformation begins with the formation of shear bands that are activated by the movement of individual free volume or collective movement of loosely packed atomic sites and is strongly related with potential STZ sites [55]. Thus, the more numbers of potential STZ sites, the higher degree of inhomogeneity, and the larger plasticity of metallic glasses will get. Besides, for the $Fe_{56}Ni_{20}Mo_4P_{12}C_4B_4$ BMG, the Poisson's ratio of the alloy system can be increased by Ni addition, since Ni has higher Poisson's ratio (0.31) compared with Fe (0.29) [31]. It is known that the higher Poisson's ratio is accompanied by more number of potential STZ sites [56,57], resulting in an increasing number of secondary shear bands arising during deformation, thus the improved plasticity.

Then, proper addition of Si element in the $Fe_{56}Ni_{20}Mo_4P_{12}C_4B_4$ BMG further improves the plastic strain up to 7%. As seen in Fig. 4(b) and (c), although both curves of two Fe-based BMGs exhibit obvious serrated flow behavior, the serration patterns are different with addition of Si element, which indicates changes in shear-band dynamics of $Fe_{56}Ni_{20}Mo_4P_{12}C_4B_4$ and $Fe_{56}Ni_{20}Mo_4P_{11}C_4B_4Si_1$ BMGs. A detailed analysis of serration patterns will be given as follows. As seen in Fig. 6(a), the serrated process is characterized by repeated cycles consisting of a sudden stress drop and a gradual rising section. It is believed that the stress drop section stands for the formation and expansion processes of the shear bands, while the rising section represents the elastic loading process. As shown in Fig. 6(b), the duration time (t_p) of stress drop is shorter than the elastic loading time (t_e). It means that the energy slowly accumulates forming shear bands. When the formation

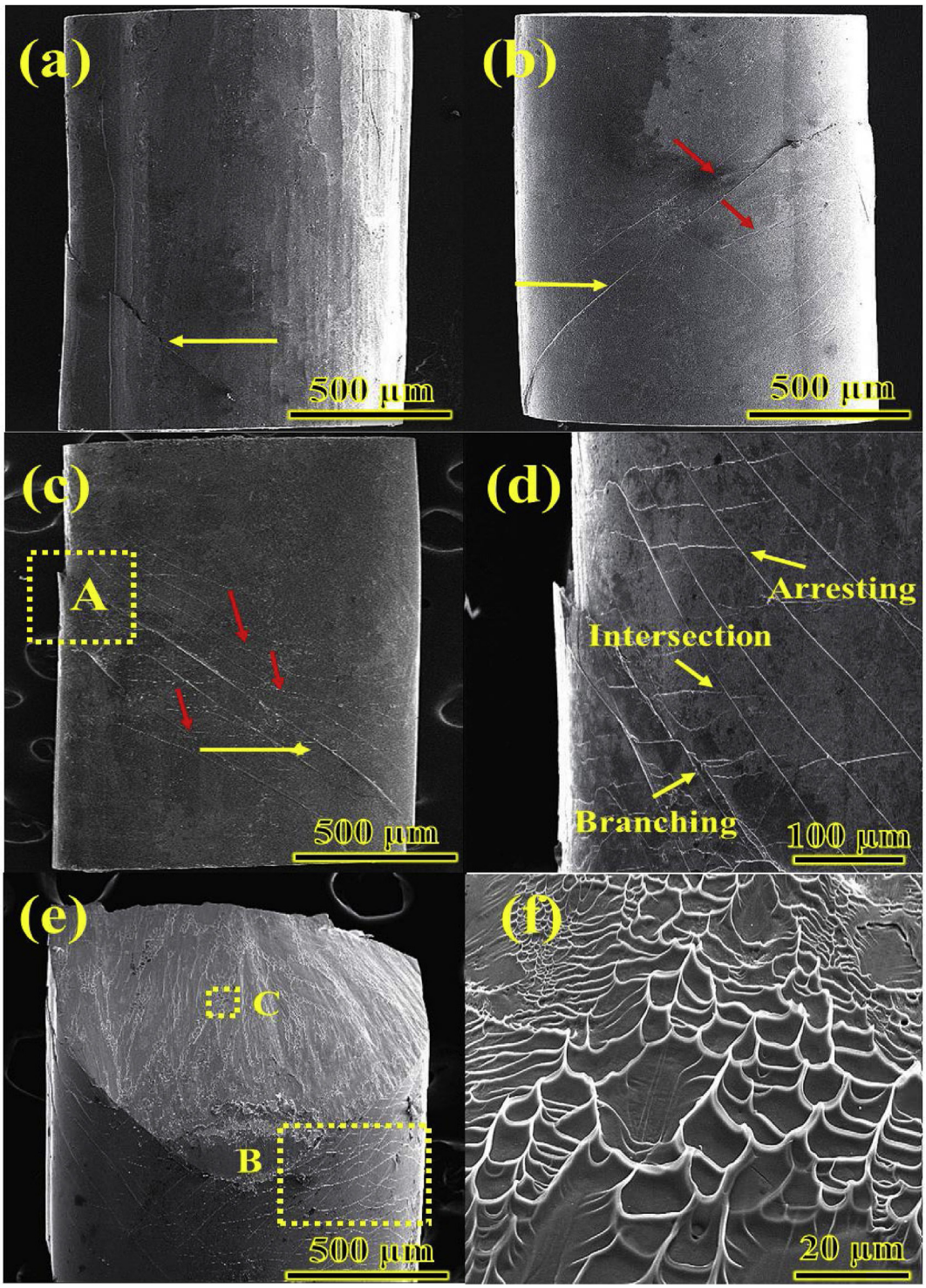

Fig. 5. SEM images taken from the deformed and fractured $Fe_{76-x}Ni_xMo_4P_{12-y}C_4B_4Si_y$ (x = 0, 10, 20; y = 0, 1, 2 at. %) samples: (a) The shear band morphology of $Fe_{76}Mo_4P_{12}C_4B_4$ BMG after deformation. (b) The shear band morphology of $Fe_{56}Ni_{20}Mo_4P_{12}C_4B_4$ BMG after deformation. (c) The shear band morphology of ductile $Fe_{56}Ni_{20}Mo_4P_{11}C_4B_4Si_1$ BMG after deformation. (d) The magnified region A in (c) showing the intersection, arresting and branching between multiple shear bands. (e) The fractured surface of $Fe_{56}Ni_{20}Mo_4P_{11}C_4B_4Si_1$ BMG. (f) Vein patterns for $Fe_{56}Ni_{20}Mo_4P_{11}C_4B_4Si_1$ BMG after failure (enlarged region C in (e)).

process finished, the shear bands expand rapidly to release the energy. At this point in the process, the stress drop magnitude is denoted as stress-drop magnitude ($\triangle\sigma_s$), which is calculated from the difference between the maximum and minimum of each serration. This drop reflects the slippage size of shear band and depends heavily on the plasticity of this Fe-based BMGs system.

The statistics results of serrations in $Fe_{56}Ni_{20}Mo_4P_{12}C_4B_4$ and $Fe_{56}Ni_{20}Mo_4P_{11}C_4B_4Si_1$ BMGs are shown in Fig. 7. Each point in Fig. 7 represents a serration on the loading curves. The horizontal axis represents the time when the serration occurs, and the vertical axis represents the $\triangle\sigma_s$ of the serrations. Considering the machine error, the serrations with a size less than 1 MPa are not counted. For

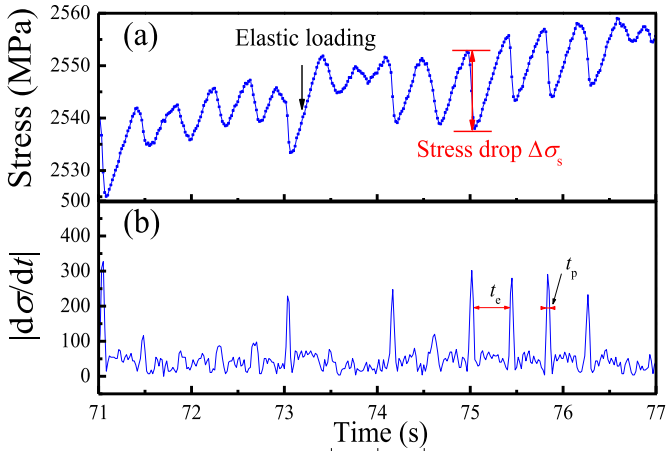

Fig. 6. (a) Stress vs. time curve for $Fe_{56}Ni_{20}Mo_4P_{11}C_4B_4Si_1$ BMG. (b) The absolute derivative of the stress versus time from (a), which shows the t_e and t_p of a single serration.

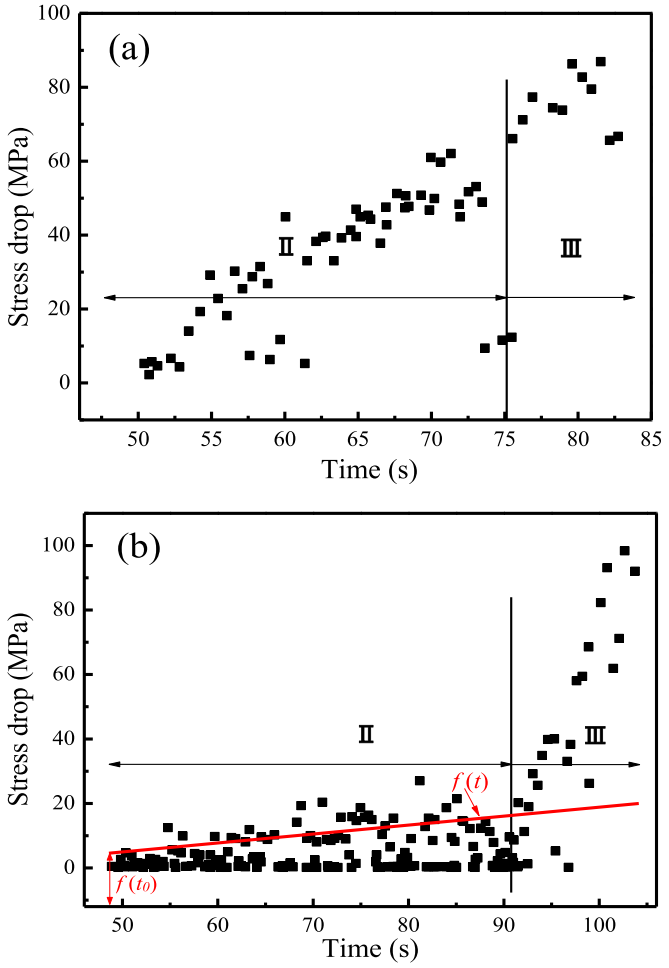

Fig. 7. The curves of stress drop with time for (a) $Fe_{56}Ni_{20}Mo_4P_{12}C_4B_4$ BMG and (b) $Fe_{56}Ni_{20}Mo_4P_{11}C_4B_4Si_1$ BMG. The red line is the average stress drop obtained by the linear regression fit. (For interpretation of the references to colour in this figure legend, the reader is referred to the Web version of this article.)

the $Fe_{56}Ni_{20}Mo_4P_{12}C_4B_4$ BMG, the $\triangle\sigma_s$ increases linearly with time during stage II and III from 1 to 90 MPa, and a few small $\triangle\sigma_s$ could be observed, as seen in Fig. 7(a). For the $Fe_{56}Ni_{20}Mo_4P_{11}C_4B_4Si_1$ BMG, $\triangle\sigma_s$ grows slowly with time in stage II, then increases drastically in stage III, as seen in Fig. 7(b). It can be seen that a large number of small $\triangle\sigma_s$ with a size less than 10 MPa could be observed during the whole stage II period, and large $\triangle\sigma_s$ above 30 MPa could only be observed in stage III.

To further reveal the underlying dynamics of serrated flow behavior, the distribution histograms of the $\triangle\sigma_s$ of $Fe_{56}Ni_{20}Mo_4P_{12}C_4B_4$ and $Fe_{56}Ni_{20}Mo_4P_{11}C_4B_4Si_1$ BMGs are shown in Fig. 8. As shown in Fig. 8(a), one can see that the histograms of the $Fe_{56}Ni_{20}Mo_4P_{12}C_4B_4$ BMG display a peak shape with most stress drops concentrated in the range of 40 MPa–60 MPa, indicating that the serration size of the $Fe_{56}Ni_{20}Mo_4P_{12}C_4B_4$ BMG has a characteristic length scale. This is consistent with the recent studies on the serrated flow dynamics where the primary shear band has chaotic dynamics with a Gaussian-like peak distribution of serrations [32]. In contrast, the serration patterns of the $Fe_{56}Ni_{20}Mo_4P_{11}C_4B_4Si_1$ BMGs are much more complex and display a monotonically decreasing distribution, as seen in Fig. 8(b), indicating that the fundamental dynamics of shear banding has changed with addition of Si element. To quantify this behavior, the inset of Fig. 8(b) gives the power spectrum $S(\omega)$, obtained by Fourier transformation on stress-time curve. Here, the $S(\omega)$ for the $Fe_{56}Ni_{20}Mo_4P_{11}C_4B_4Si_1$ BMG can be well described by a power-law

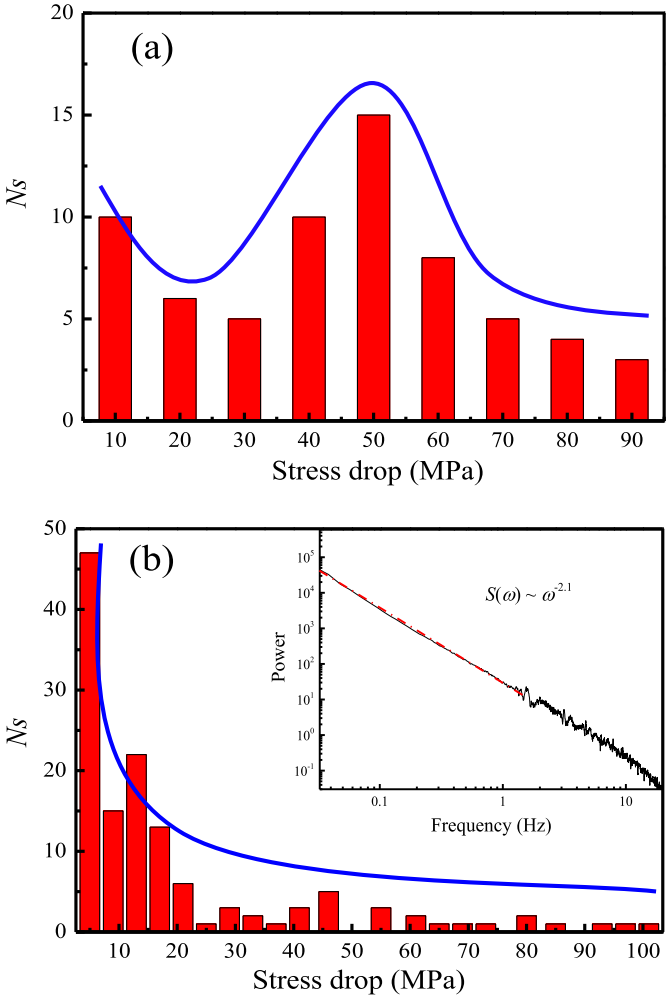

Fig. 8. The statistical distribution of frequency calculated from the continuous strain-stress curves of plastic deformations for (a) $Fe_{56}Ni_{20}Mo_4P_{12}C_4B_4$ BMG and (b) $Fe_{56}Ni_{20}Mo_4P_{11}C_4B_4Si_1$ BMG. The inset represent the corresponding power spectrum $S(\omega) \sim \omega$ for $Fe_{56}Ni_{20}Mo_4P_{11}C_4B_4Si_1$ BMG.

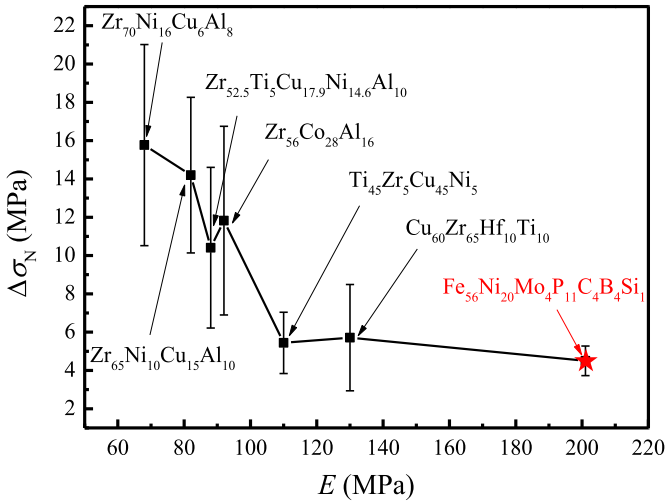

Fig. 9. The variation of the mean stress drop magnitude $\triangle\sigma_N$ with the Young's modulus E for different BMGs.

distribution $S(\omega) \sim \omega^{-\alpha}$, where $\alpha \approx 2.1$. This power-law relation is an indicator of the SOC state in dynamics [32,58], which means that the system can buffer against large changes (not completely immune) and endure intervention from any external impact on such a complex system, that can be dissipated throughout the networks of connected participants [59,60]. Thus, it is obvious that the shear-band dynamics of the $Fe_{56}Ni_{20}Mo_4P_{12}C_4B_4$ and $Fe_{56}Ni_{20}Mo_4P_{11}C_4B_4Si_1$ BMGs changes from chaos to SOC state.

In addition, the stability of shear bands is also an important factor for the plasticity of Fe-based BMGs, which may be tightly linked to the shear-band dynamics. We use the normalized serration size $\triangle\sigma_N$ to measure the shear band stability in this Fe-based BMGs system, because the size of serrations could represent the sliding distance [61]. As seen in Fig. 7 (b), using a linear regression fit through the stress drop *vs.* time diagram, $\overline{\triangle\sigma s} = f(t)$, and then the mean stress drop is normalized by:

$$\Delta\sigma_N = \Delta\sigma_S/[f(t)/f(t_0)] \quad (1)$$

Where $f(t_0)$ is the fitted value at the starting time t_0. After such normalization, the $\triangle\sigma_N$ of 4.5 MPa for $Fe_{56}Ni_{20}Mo_4P_{11}C_4B_4Si_1$ BMG are obtained. We further compared the $\triangle\sigma_N$ of $Fe_{56}Ni_{20}Mo_4P_{11}C_4B_4Si_1$ BMG to the data of the other glassy alloys, which were reported by Hu et al. [62]. As shown in Fig. 9, a decrease trend can be found for the $\triangle\sigma_N$ with increasing E. As reported by Hu et al. the stiffer the BMG, the smaller the shear event is [62]. And similar trend was recently reported by Ke et al. [41] in the micro compression tests of different metallic glasses. Clearly, the $\triangle\sigma_N$ of this stiffer $Fe_{56}Ni_{20}Mo_4P_{11}C_4B_4Si_1$ BMG is smaller than any other BMGs, suggesting extraordinary stable shear-band dynamics in the $Fe_{56}Ni_{20}Mo_4P_{11}C_4B_4Si_1$ BMG. The stable shear-band dynamics represents the low possibility of fracture in a single shear band, resulting in a strong tendency of forming shear band interactions. And the shear band interactions mean that all shear bands involved in the deformation, rendering the propagation of shear bands more difficult, causing an evolvement of the shear-band dynamics to the SOC state. The multiple shear bands observed in the outer and fractured surfaces further confirm that the $Fe_{56}Ni_{20}Mo_4P_{11}C_4B_4Si_1$ BMG deforms by a large number of small stress-drop serrations in SOC dynamics.

Based on the theory of inhomogeneity, we can infer that the formation of multiple shear bands with Si addition is due to the increase of potential STZ sites. To verify this opinion, the structural changes in Fe-based BMGs were investigated. As shown in the XRD results, the principal diffraction angle (2θ) decreases with the addition of Si element. According to the Bragg equation: $\lambda = 2r_1\sin\theta$, a decrease in θ represents an increase in average atomic distance, resulting in a loose structure and large free volume in Fe-based BMGs. In addition, since the atomic sizes of the metalloids change in the order of Si > P > B > C, the dissolution of Si with larger atomic size will increase the internal stress [47]. Indeed, recent

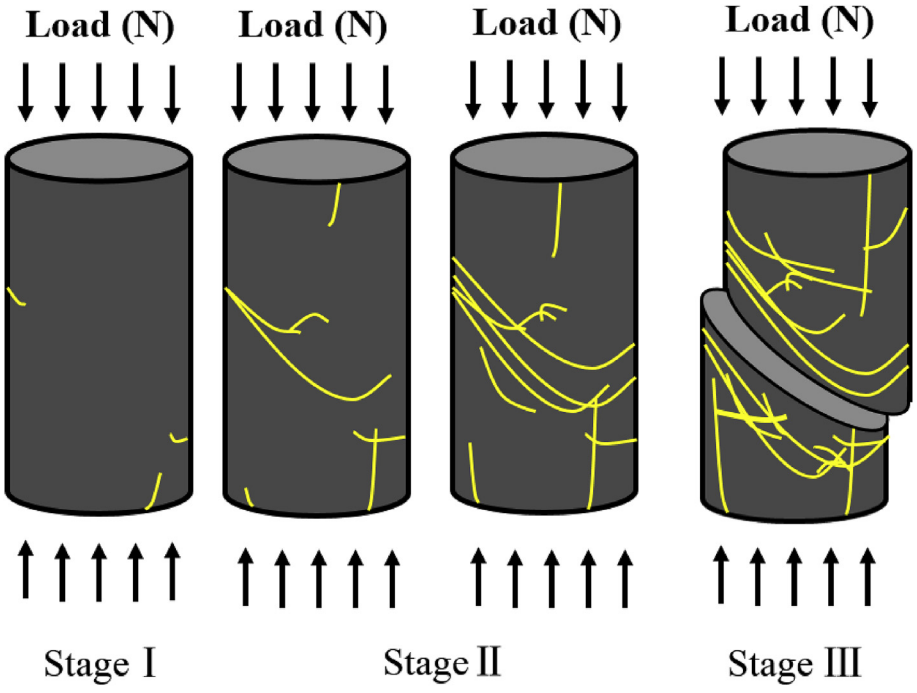

Fig. 10. Schematic diagram illustrating the shear-band dynamics in the ductile $Fe_{56}Ni_{20}Mo_4P_{11}C_4B_4Si_1$ BMG.

studies suggested that STZ is more likely to be found in local regions having certain structural features, e.g. areas with loosely packed atomic sites [63], large free volume [64] and under higher atomic-level stresses [55,65]. These regions can therefore be treated as plausible sites for STZ formation in BMGs. Thus, potential STZ sites were increased with the addition of Si element, leading to the formation of multiple shear bands during deformation. As a result, the plasticity was improved.

To better understand how shear bands propagates in these ductile Fe-based BMGs in SOC dynamics, schematic diagram illustrating the motion of shear bands of $Fe_{56}Ni_{20}Mo_4P_{11}C_4B_4Si_1$ BMG is shown in Fig. 10. In the elastic deformation stage (stageI), the potential STZ sites in BMGs grow constantly with increasing applied stress. During the later serration process (stageII), both propagation of old shear bands and formation of new shear bands can be activated. If the later shear bands could propagate along a direction different from the former shear bands, the shear band interactions will be formed. The interaction of multiple shear bands favors the efficient dissipation of accumulated elastic energy by a homogeneous distribution of strain and thus prevents early catastrophic failure along a single shear band [66]. In addition, new potential STZ sites will be formed due to the stress concentration at the interactions. Therefore, the serration and multiplication process could sustain, resulting in a stable plastic deformation region. After that, once the primary shear band evolves into a crack and the sample begins to slip along the main shear plane, large serrations occur accompanied with decreasing stress in stage III. Although the primary shear band takes a portion of the overall plastic strain, the obvious intersection and arresting phenomenon of secondary shear bands indicate that the plastic strain is also related with formation of new shear bands. Under this understanding, the plasticity of Fe-based BMGs apparently correlates with the ability of forming shear band interactions, which is related to the degree of inhomogeneity.

4. Conclusions

FeNiMoPCBSi BMGs system with high GFA and excellent soft magnetic as well as high strength and large plastic strain were successfully synthesized. The reasons of improved plasticity and varied serration behaviors with different Ni and Si additions were detailed discussed, which provides new experimental evidences for different shear-band dynamics in Fe-based BMGs with different plasticity. The results obtained are summarized as follows:

(1) The critical diameter for glass formation of the $Fe_{76-x}Ni_xMo_4P_{12-y}C_4B_4Si_y$ BMGs is 2 mm. This glassy alloy system exhibits excellent soft magnetic properties with relatively high B_s of 0.88–1.10 T and low H_c of 1.0–1.9 A/m.
(2) Proper additions of Ni and Si elements are effective to improve the plasticity of Fe-based BMGs. Substitution of 20 at. % Ni for Fe, combined with 1 at. % Si addition in the $Fe_{76-x}Ni_xMo_4P_{12-y}C_4B_4Si_y$ BMGs dramatically improves the plastic strain from 1.7 to 7%.
(3) The serrated flow behavior is not observed in the $Fe_{76}Mo_4P_{12}C_4B_4$ BMG. However, the chaos state occurs in the $Fe_{56}Ni_{20}Mo_4P_{12}C_4B_4$ BMG, and eventually the SOC behavior appears in the $Fe_{56}Ni_{20}Mo_4P_{11}C_4B_4Si_1$ BMG.
(4) The $Fe_{76}Mo_4P_{12}C_4B_4$ BMG deforms through a single shear band movement, exhibiting poor plasticity. For the $Fe_{56}Ni_{20}Mo_4P_{12}C_4B_4$ BMG, a few secondary shear bands occur around the primary shear band, propagating randomly in chaotic dynamics. But for the $Fe_{56}Ni_{20}Mo_4P_{11}C_4B_4Si_1$BMG, multiple shear bands form and interact with each other following the SOC dynamics, leading to large plastic strain. The improved plasticity of this Fe-based BMG might result from more inhomogeneity, caused by the increasing number of potential STZ sites.

Acknowledgement

This work was supported by the National Natural Science Foundation of China (Grant Nos. 51631003, 51671121, 51501037and 51871237) and the Fundamental Research Funds for the Central Universities (Grant No. 2242016K41001).

References

[1] P. Duwez, S.C.H. Lin, Amorphous ferromagnetic phase in iron-carbon-phosphorus alloys, J. Appl. Phys. 38 (1967) 4096–4097.
[2] K.L. Alvarez, J.M. Martín, M. Ipatov, J. Gonzalez, Soft magnetic amorphous alloys (Fe-rich) obtained by gas atomization technique, J. Alloys Compd. 735 (2018) 2646–2652.
[3] R. Hasegawa, Applications of amorphous magnetic alloys, Mater. Sci. Eng. A 375 (2004) 90–97.
[4] C. Suryanarayana, A. Inoue, Iron-based bulk metallic glasses, Int. Mater. Rev. 58 (2013) 131–166.
[5] A. Inoue, F.L. Kong, Y. Han, S.L. Zhu, A. Churyumov, E. Shalaan, Development and application of Fe-based soft magnetic bulk metallic glassy inductors, J. Alloys Compd. 731 (2018) 1303–1309.
[6] V.S. Raja, Kishore, S. Ranganathan, Crystallization behavior of Metglas 2826 MB ($Fe_{40}Ni_{38}Mo_4B_{18}$), Bull. Mater. Sci. 9 (1987) 207–217.
[7] A. Inoue, Y. Shinohara, J.S. Gook, Thermal and magnetic properties of bulk Fe-based glassy alloys prepared by copper mold casting, Mater. Trans. JIM 36 (1995) 1427–1433.
[8] Z.P. Lu, C.T. Liu, J.R. Thompson, W.D. Porter, Structural amorphous steels, Phys. Rev. Lett. 92 (2004), 245503.
[9] V. Ponnambalam, S.J. Poon, G.J. Shiflet, Fe-based bulk metallic glasses with diameter thickness larger than one centimeter, J. Mater. Res. 19 (2004) 1320–1323.
[10] D.H. Kim, J.M. Park, D.H. Kim, W.T. Kim, Development of quaternary Fe–B–Y–Nb bulk glassy alloys with high glass-forming ability, J. Mater. Res. 22 (2007) 471–477.
[11] J.H. Yao, J.Q. Wang, Y. Li, Ductile Fe-Nb-B bulk metallic glass with ultrahigh strength, Appl. Phys. Lett. 92 (2008), 251906.
[12] J.H. Zhang, C.T. Chang, A.D. Wang, B.L. Shen, Development of quaternary Fe-based bulk metallic glasses with high saturation magnetization above 1.6 T, J. Non-Cryst. Solids 358 (2012) 1443–1446.
[13] T. Paul, N. Chawake, R.S. Kottada, S.P. Harimkar, Pressure controlled micro-viscous deformation assisted spark plasma sintering of Fe-based bulk amorphous alloy, J. Alloys Compd. 738 (2018) 10–15.
[14] J.J. Si, C.X. Du, T. Wang, Y.D. Wu, R.S. Wang, X.D. Hui, Glass formation and soft magnetic properties of novel Fe-rich Fe-B-Ti-Zr bulk metallic glasses, J. Alloys Compd. 741 (2018) 542–548.
[15] Y.X. Geng, X. Lin, J. Li, S.M. Fan, H.B. Ju, L.H. Yu, J.H. Xu, Y.M. Wang, Super-high hardness of (Fe,Co)-B-Si-Zr/Hf bulk glassy alloys, J. Alloys Compd. 753 (2018) 351–355.
[16] C.T. Chang, B.L. Shen, A. Inoue, FeNi-based bulk glassy alloys with superhigh mechanical strength and excellent soft-magnetic properties, Appl. Phys. Lett. 89 (2006), 051912.
[17] A.D. Wang, M.X. Zhang, J.H. Zhang, H. Men, B.L. Shen, S.J. Pang, T. Zhang, FeNiPBNb bulk glassy alloys with good soft-magnetic properties, J. Alloys Compd. 536 (2012) S354–S358.
[18] A. Inoue, B.L. Shen, A new Fe-based bulk glassy alloy with outstanding mechanical properties, Adv. Mater. 16 (2004) 23–24.
[19] B.L. Shen, H. Men, A. Inoue, Fe-based bulk glassy alloy composite containing in situ formed α-(Fe,Co) and $(Fe,Co)_{23}B_6$ microcrystalline grains, Appl. Phys. Lett. 89 (2006), 101915.
[20] K.F. Yao, C.Q. Zhang, Fe-based bulk metallic glass with high plasticity, Appl. Phys. Lett. 90 (2007), 061901.
[21] J.M. Park, G. Wang, R. Li, N. Mattern, J. Eckert, D.H. Kim, Enhancement of plastic deformability in Fe-Ni-Nb-B bulk glassy alloys by controlling the Ni-to-Fe concentration ratio, Appl. Phys. Lett. 96 (2010), 031905.
[22] S.F. Guo, L. Liu, N. Li, Y. Li, Fe-based bulk metallic glass matrix composite with large plasticity, Scripta Mater. 62 (2010) 329–332.
[23] A. Seifoddini, M. Stoica, M. Nili-Ahmadabadi, S. Heshmati-Manesh, U. Kuhn, J. Eckert, New $(Fe_{0.9}Ni_{0.1})_{77}Mo_5P_9C_{7.5}B_{1.5}$ glassy alloys with enhanced glass-forming ability and large compressive strain, Mater. Sci. Eng. A 560 (2013) 575–582.
[24] M. Stoica, S. Scudio, J. Bednarcik, I. Kaban, J. Eckert, FeCoSiBNbCu bulk metallic glass with large compressive deformability studied by time-resolved synchrotron X-ray diffraction, J. Appl. Phys. 115 (2014), 053520.
[25] P. Rezaei-Shahreza, A. Seifoddini, S. Hasani, Microstructural and phase evolutions: their dependent mechanical and magnetic properties in a Fe-based amorphous alloy during annealing process, J. Alloys Compd. 738 (2018) 197–205.
[26] G.L. Zhang, Q.Q. Wang, C.C. Yuan, W.M. Yang, J. Zhou, L. Xue, F. Hu, B.A. Sun,

B.L. Shen, Effects of Cu additions on mechanical and soft-magnetic properties of CoFeBSiNb bulk metallic glasses, J. Alloys Compd. 737 (2018) 815–820.
[27] M. Stoica, P. Ramasamy, I. Kaban, S. Scudino, M. Nicoara, G.B.M. Vaughan, J. Wright, R. Kumar, J. Eckert, Structure evolution of soft magnetic $(Fe_{36}Co_{36}B_{19.2}Si_{4.8}Nb_4)_{100-x}Cu_x$ (x = 0 and 0.5) bulk glassy alloys, Acta Mater. 95 (2015) 335–342.
[28] J.J. Lewandowski, W.H. Wang, A.L. Greer, Intrinsic plasticity or brittleness of metallic glasses, Phil. Mag. Lett. 85 (2005) 77–87.
[29] S.F. Guo, J.L. Qiu, P. Yu, S.H. Xie, W. Chen, Fe-based bulk metallic glasses: brittle or ductile? Appl. Phys. Lett. 105 (2014), 161901.
[30] W.M. Yang, H.S. Liu, Y.C. Zhao, A. Inoue, K.M. Jiang, J.T. Hou, H.B. Ling, Q. Li, B.L. Shen, Mechanical properties and structural features of novel Fe-based bulk metallic glasses with unprecedented plasticity, Sci. Rep. 4 (2014) 6233.
[31] Y.Q. Cheng, A.J. Cao, E. Ma, Correlation between the elastic modulus and the intrinsic plastic behavior of metallic glasses: the roles of atomic configuration and alloy composition, Acta Mater. 571 (2009) 3253–3267.
[32] B.A. Sun, H.B. Yu, W. Jiao, H.Y. Bai, D.Q. Zhao, W.H. Wang, Plasticity of ductile metallic glasses: a self-organized critical state, Phys. Rev. Lett. 105 (2010), 035501.
[33] J.W. Qiao, F.Q. Yang, G.Y. Wang, P.K. Liaw, Y. Zhang, Jerky-flow characteristics for a Zr-based bulk metallic glass, Scr. Mater. 63 (2010) 1081–1084.
[34] R. Maaß, J.F. Löffler, Shear-band dynamics in metallic glasses, Adv. Funct. Mater. 23 (2015) 2353–2368.
[35] W.M. Yang, B.A. Sun, Y.C. Zhao, Q. Li, L. Hou, N. Luo, C.C. Dun, C.L. Zhao, Z.G. Ma, H.S. Liu, B.L. Shen, Non-repeatability of large plasticity for Fe-based bulk metallic glasses, J. Alloys Compd. 676 (2016) 209–214.
[36] V. Venkatesh, Gouthama, K. Mondal, Effect of cast temperature, size and annealing condition on the serrated flow during nano-indentation of Zr-based bulk metallic glasses, J. Alloys Compd. 692 (2017) 745–757.
[37] R. Rashidi, M. Malekan, Y. Hamishebahar, Serration dynamics in the presence of chemical heterogeneities for a Cu-Zr based bulk metallic glass, J. Alloys Compd. 775 (2018) 298–303.
[38] E.V. Boltynjuk, D.V. Gunderov, E.V. Ubyivovk, M.A. Monclús, L.W. Yang, J.M. Molina-Aldareguia, A.L. Tyurin, A.R. Kilmametov, A.A. Churakova, A.Yu. Churyumov, R.Z. Valiev, Enhanced strain rate sensitivity of Zr-based bulk metallic glasses subjected to high pressure torsion, J. Alloys Compd. 747 (2018) 595–602.
[39] H. Huang, M.Q. Jiang, J.W. Yan, The coupling effects of laser thermal shock and surface nitridation on mechanical properties of Zr-based metallic glass, J. Alloys Compd. 770 (2018) 864–874.
[40] B.A. Sun, S. Pauly, J. Tan, M. Stoica, W.H. Wang, U. Kühn, J. Eckert, Serrated flow and stick–slip deformation dynamics in the presence of shear-band interactions for a Zr-based metallic glass, Acta Mater. 60 (2012) 4160–4171.
[41] H.B. Ke, B.A. Sun, C.T. Liu, Y. Yang, Effect of size and base-element on the jerky flow dynamics in metallic glass, Acta Mater. 63 (2014) 180–190.
[42] G.N. Yang, J.L. Gu, S.Q. Chen, Y. Shao, H. Wang, K.F. Yao, Serration behavior of a Zr-based metallic glass under different constrained loading conditions, Metall. Mater. Trans. A 47A (2016) 5395–5400.
[43] J.W. Qiao, Y. Zhang, P.K. Liaw, Serrated flow kinetics in a Zr-based bulk metallic glass, Intermetallics 18 (2010) 2057–2064.
[44] J. Antonaglia, X. Xie, G. Schwarz, M. Wraith, J. Qiao, Y. Zhang, P.K. Liaw, J.T. Uhl, K.A. Dahmen, Tuned critical avalanche scaling in bulk metallic glasses, Sci. Rep. 4 (2014) 4382.
[45] L.H. Liu, Z.Y. Liu, Y. Huan, X.Y. Wu, Y. Lou, X.S. Huang, L.J. He, P.J. Li, L.C. Zhang, Effect of structural heterogeneity on serrated flow behavior of Zr-based metallic glass, J. Alloys Compd. 766 (2018) 908–917.
[46] J. Zhou, W.M. Yang, C.C. Yuan, B.A. Sun, B.L. Shen, Ductile FeNi-based bulk metallic glasses with high strength and excellent soft magnetic properties, J. Alloys Compd. 742 (2018) 318–324.
[47] B.L. Shen, A. Inoue, Bulk glassy Fe–Ga–P–C–B–Si alloys with high glass-forming ability, high saturation magnetization and good soft magnetic properties, Mater. Trans. 43 (2002) 1235–1239.
[48] B.L. Shen, M. Akiba, A. Inoue, Excellent soft-ferromagnetic bulk glassy alloys with high saturation magnetization, Appl. Phys. Lett. 88 (2006), 131907.
[49] B.L. Shen, M. Akiba, A. Inoue, Effects of Si and Mo additions on glass-forming in FeGaPCB bulk glassy alloys with high saturation magnetization, Phys. Rev. B 73 (2006), 104204.
[50] F.S. Li, B.L. Shen, A. Makino, A. Inoue, Excellent soft-magnetic properties of (Fe,Co)–Mo–(P,C,B,Si) bulk glassy alloys with ductile deformation behavior, Appl. Phys. Lett. 91 (2007), 234101.
[51] A. Takeuchi, A. Inoue, Classification of bulk metallic glasses by atomic size difference, heat of mixing and period of constituent elements and its application to characterization of the main alloying element, Mater. Trans. 46 (2005) 2817–2829.
[52] M. Mitera, M. Naka, T. Masumoto, N. Kazama, H. Watanabe, Effects of metalloids on magnetic-properties of iron based amorphous alloys, Phys. Status Solidi (a) 49 (1978) K163–K166.
[53] Metal Databook, fourth ed., Japan Institute of Metal, Maruzen, 2004, p. 8.
[54] J.W. Qiao, H.L. Jia, Y. Zhang, P.K. Liaw, L.F. Li, Multi-step shear banding for bulk metallic glasses at ambient and cryogenic temperature, Mater. Chem. Phys. 136 (2012) 75–79.
[55] A.L. Greer, Y.Q. Cheng, E. Ma, Shear bands in metallic glasses, Mater. Sci. Eng. R 74 (2013) 71–132.
[56] D. Pan, A. Ionue, T. Sakurai, M.W. Chen, Experimental characterization of shear transformation zones for plastic flow of bulk metallic glasses, Proc. Natl. Acad. Sci. U.S.A. 105 (2008) 14769–14772.
[57] J.S. Langer, Dynamics of shear-transformation zones in amorphous plasticity: formulation in terms of an effective disorder temperature, Phys. Rev. E 70 (2004), 041502.
[58] P. Sammonds, Deformation dynamics-plasticity goes supercritical, Nat. Mater. 4 (2005) 425–426.
[59] G. Wang, K.C. Chan, L. Xia, P. Yu, J. Shen, W.H. Wang, Self-organized intermittent plastic flow in bulk metallic glasses, Acta Mater. 57 (2009) 6146–6155.
[60] Z. Wang, J.W. Qiao, H.J. Yang, P.K. Liaw, C.J. Huang, L.F. Li, Serration dynamics in a Zr-based bulk metallic glass, Metall. Mater. Trans. A 46A (2014) 2404–2414.
[61] G.N. Yang, S.Q. Chen, J.L. Gu, S.F. Zhao, J.F. Li, Y. Shao, H. Wang, K.F. Yao, Serration behaviours in metallic glassed with different plasticity, Philos. Mag. 96 (2016) 1–13.
[62] J. Hu, B.A. Sun, Y. Yang, C.T. Liu, S. Pauly, Y.X. Weng, J. Eckert, Intrinsic versus extrinsic effects on serrated flow of bulk metallic glasses, Intermetallics 66 (2015) 31–39.
[63] A.S. Argon, Plastic deformation in metallic glasses, Acta Metall. 27 (1979) 47–58.
[64] F. Delogu, Identification and characterization of potential shear transformation zones in metallic glasses, Phys. Rev. Lett. 100 (2008), 255901.
[65] D. Srolovitz, V. Vitek, T. Egami, An atomistic study of deformation of amorphous metals, Acta Mater. 31 (1983) 335–352.
[66] Y.H. Liu, C.T. Liu, A. Gali, A. Inoue, M.W. Chen, Evolution of shear bands and its correlation with mechanical response of a ductile $Zr_{55}Pd_{10}Cu_{20}Ni_5Al_{10}$ bulk metallic glass, Intermetallics 18 (2010) 1455–1464.